IOP Publishing Phys. Med. Biol. 65 (2020) 015012 (15pp) https://doi.org/10.1088/1361-6560/ab5c47

Physics in Medicine & Biology

IPEM Institute of Physics and Engineering in Medicine

PAPER

RECEIVED
22 June 2019

REVISED
11 November 2019

ACCEPTED FOR PUBLICATION
27 November 2019

PUBLISHED
13 January 2020

Small-field dosimetry with a high-resolution 3D scanning water phantom system for the small animal radiation research platform SARRP: a geometrical and quantitative study

Erika Muñoz Arango[1], José Guilherme Peixoto[1,2] and Carlos Eduardo de Almeida[1]

[1] Laboratório de Ciências Radiológicas, Universidade do Estado do Rio de Janeiro, RJ, Brazil
[2] Laboratório Nacional de Metrologia das Radiações Ionizantes, LNMRI-IRD, Rio de Janeiro, RJ, Brazil

E-mail: munozare@gmail.com

Keywords: preclinical radiotherapy, small kV fields dosimetry, ionization chambers, solid-state detectors, small animal radiation research platform (SARRP)

Abstract

Improvements in dosimetry in preclinical radiation research facilitate the application of results to the newest radiotherapy techniques, reducing gaps that hinder translation. Currently, guidelines for small-field kV photon dosimetry of small animal irradiators have not been published, and most of the publications are based on radiochromic film dosimetry. In this study, we evaluated the performance of four detectors, three ionization chambers (ICs): (PTW Advanced Markus, PTW Semiflex 31010, PTW PinPoint-3D 31016) and one solid-state detector (PTW 60017 unshielded Diode E) regarding their suitability for relative dosimetry of the small animal radiation research platform SARRP (220 kVp). The measurements were performed in a high-resolution 3D scanning phantom, centering the detectors in the field following the in-plane and cross-plane profiles method at two depths. Depth dose curves (PDDs) and profiles were measured in water for field sizes ranging from $40 \times 40\,mm^2$ to $5 \times 5\,mm^2$. Quantitative analysis was performed through global and local dose differences (DDs) between the PDDs and the Advanced Markus parallel plate IC data and through the gamma index (γ) criteria for profiles compared against data from EBT3 films provided by the manufacturer. Compared to the Advanced Markus IC, the PDD results suggest that PinPoint-3D is suitable for depth measurements at this beam quality, even near the surface, with agreements better than 1%. Semiflex 31010 was accurate to within 1.5% for measurements deeper than 5 mm. Diode E showed a dramatic DD and should not be recommended for the field sizes and kVp evaluated in this study. In agreement with γ analyses, PinPoint-3D and Diode E are good candidates for profile measurements of field sizes from $40 \times 40\,mm^2$ to $10 \times 10\,mm^2$. For $5 \times 5\,mm^2$ profiles, only Diode E showed good results, making it a recommended detector for profile measurements.

1. Introduction

Radiotherapy technological advances with hypofractionated techniques of small fields have evolved faster than the possibility of research in radiobiology and preclinical fields, which has encouraged the development of modern micro irradiator systems for small animals (Verhaegen *et al* 2011, 2018, Bazalova *et al* 2013). In radiobiological studies, dosimetric procedures should be as close as possible to the recommendations in the clinical radiation dosimetry, ensuring high accuracy and precision of the delivered dose, increasing the chance of achieving translatable results (Liu *et al* 2013, Verhaegen *et al* 2018, Muñoz *et al* 2019) and reducing the gaps between preclinical and clinical research (Desrosiers *et al* 2013, Mijnheer 2018).

There are currently two commercial microirradiators that have been more widely distributed: the Small Animal Radiation Research Platform (SARRP, Xstrahl Ltd, Camberley, UK) and XRAD225Cx (PXI North Branford, CT, USA). These systems with x-ray photon beams of medium energy (200–225 kVp) and field sizes of a few mm present challenges in terms of the small-field dosimetry. Commissioning procedures for these systems are mainly manufacturer dependent, and a code of practice (CoP) or specific recommendations for relative dosimetry are

not available at present (Mijnheer 2018). Small-field commissioning studies for the kV medium energy range have been described in other publications, where dosimetry is mainly based on solid water phantoms, ionization chambers for reference dosimetry (Wong *et al* 2008, Tryggestad *et al* 2009, Newton *et al* 2011, Pidikiti *et al* 2011, Lindsay *et al* 2014) and radiochromic film dosimeters, with some difficulties to handling reported (Villarreal-Barajas and Khan 2014, Mijnheer 2018, Wang *et al* 2018).

Some protocols have been published to date orienting the small-field dosimetry for MV x-ray beams, for example, the IAEA TRS483: Dosimetry of small static fields used in external beam radiotherapy (IAEA 2017) and the IPEM 103 Report: Small Field MV Photon Dosimetry (IPEM 2010). These recommendations are mainly based on ionization chambers and solid-state detectors, as well as measurements carried out in water phantoms. Detectors that may be recommended and suitable for high-energy photon dosimetry may not be suitable for small fields of kV, and there is a lack of characterization at present (Johnstone *et al* 2018). One of the most important considerations to standardize in preclinical dosimetry is the definition of the small field, since; the field sizes used are even lower than in clinical radiotherapy as a consequence of the sizes of the samples (Ghita *et al* 2017, Muñoz *et al* 2019).

Currently, it is possible to find different studies showing the response of several detectors in the medium kV energy range (Ma *et al* 2001, Newton *et al* 2011, Pidikiti *et al* 2011, Hill *et al* 2014, Damodar *et al* 2018, Na *et al* 2018, Wang *et al* 2018), but the challenge of small-field dosimetry is a current discussion (Dos Santos *et al* 2018, Mijnheer 2018, Verhaegen *et al* 2018, Muñoz *et al* 2019). For x-ray beam dosimetry, vented ionization chambers have been defined as the gold standard detectors as a consequence of the small energy dependence (Hill *et al* 2014). For relative dosimetry, some ionization chambers have been widely studied and well characterized for non-small kV photon beams (Hill *et al* 2009, 2014). For high-energy small photon beams, solid-state detectors have very good properties that make them desirable for dosimetry, such as good spatial resolution, low energy response, high-efficiency collection and small sensitive volume (IPEM 2010); for kV x-ray beams, the accuracy and desirability of these detectors have a limited number of studies at present (Damodar *et al* 2018).

For small-field dosimetry, one of the challenges is the alignment of the scan arm and detector with the central axis of the beam (CAX). Errors in depth dose and profile data due to misalignment have been estimated by different authors (Cheng *et al* 2007). Reducing positioning errors and central axis deviation allows more effective analysis of the response of detectors in geometrical evaluations. Low *et al* (1998) presented the gamma index (γ) for the evaluation of dose distribution using composite acceptance criteria including dose difference (DD) and distance to agreement (DTA). The gamma index (γ) analyze has been historically used for 1D or 2D dose distribution evaluation and is widely used in commissioning and dosimetric validation processes in radiotherapy (Stojadinovic *et al* 2015, Miften *et al* 2018). The gamma index 3 mm (DTA)-3% DD is a widely used criterion in the field; however, an ideal acceptance criterion is a present discussion (Stojadinovic *et al* 2015).

In this study, we evaluated the performance of four dosimeters, three ionization chambers, and one solid-state detector regarding their suitability for relative dosimetry in water for the conformal small animal irradiator SARRP system with kilovoltage x-ray small photon fields and an applied voltage of 220 kVp. Transitional analyses between a non-small field ($40 \times 40\,mm^2$) and a small field ($5 \times 5\,mm^2$) were performed. The response of detectors was characterized to analyze dependencies in many geometrical parameters. Although several papers have reported recommendations for the relative dosimetry of SARRP (220 kVp) mainly with radiochromic film or non-small beams, we evaluated a variety of detectors, including novel models that have not been systematically investigated for the small kV photon fields in water. We evaluated the results of the dosimetry in a high-resolution 3D scanning water phantom MP3-XS (PTW, Freiburg, Germany) system and applied a very precise centralization process, centering the detectors in the field following the in-plane and cross-plane profile scans, this method was compared with the dosimetry based on a solid water phantom and radiochromic film dosimetry measured with a very specific manufacturer system Jig (Tryggestad *et al* 2009). Some recommendations for small photon beam dosimetry of MV were applied. A quantitative gamma index criterion was used in the attempt to approximate radiation oncology dosimetry analysis tools with preclinical dosimetric analysis.

2. Materials and methods

2.1. The SARRP facility

All measurements presented in this study were performed at the Small Animal Radiation Research Platform SARRP (Xstrahl Ltd, Camberley, UK) (Wong *et al* 2008) at the LCR, Rio de Janeiro State, University Brazil. The SARRP is an image-guided micro irradiator equipped with an x-ray tube of 30–220 kVp, maximum setting current of 30 mA, and a maximum isocenter dose rate of 375 cGy min^{-1} at a 1 cm depth in water for the open field. The tube (Gantry) can be rotated between 180 and $-180°$ around an isocenter point located at 35 cm from the dual focal spot (source isocenter distance). The x-ray tube specifications are inherent filtration 0.8 mm Be,

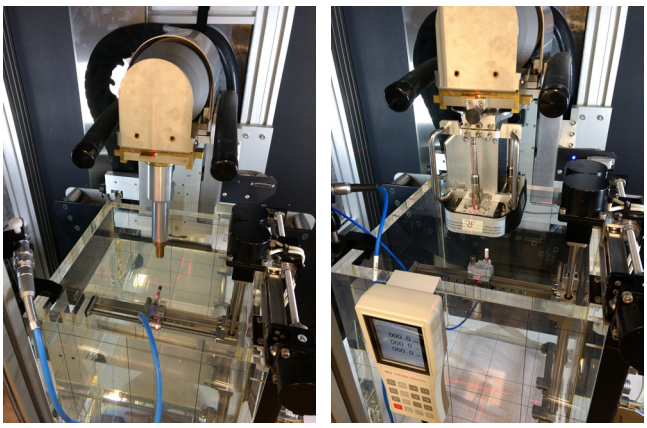

(a) (b)

Figure 1. Setup of the PTW MP3-XS system and detectors inside the SARRP cabinet. (a) Cone collimator. (b) Manual variable collimator (MVC).

1st HVL 0.634 mm Cu, calculated effective energy 64.3 keV and calculated homogeneity coefficient of 44.7%. The fall-off value ratio, proposed as the ratio of the absorbed dose to water for 20 mm and 50 mm depth $D_{2cm/5\,cm}$ (IAEA 2000), was 1.81 for a 40 × 40 mm^2 field size and source surface distance (SSD) equal to 33 cm.

The system is equipped with additional filtration of 0.15 mm copper and 1.0 mm aluminum filtration suggested for treatment and imaging modes, respectively. SARRP has a square open field size of 13.6 × 13.6 cm^2 at the isocenter and a set of interchangeable square, rectangular and circular fixed collimators, as well as an asymmetrical manual variable collimator (MVC) with rectangular or squares field sizes, ranging from 80 × 40 mm^2 to 10 × 10 mm^2. In this study, 10 × 10 mm^2, 5 × 5 mm^2 square fixed collimators and 40 × 40 mm^2 and 20 × 20 mm^2 field sizes defined with the MVC were used. For the entire study, x-ray tube parameters were fixed at 220 kVp/13 mA for treatment beam delivery, with the large 5.5 mm focal spot and the 0.15 mm Cu added filtration. Manufacturer acquisition data for commissioning of the Treatment planning system (TPS, Muriplan, Xstrahl Ltd, Camberley, UK) are based on a Farmer ionization chamber (0.6 cm^3), radiochromic EBT film dosimeter, solid water slabs and a mechanical system adhered to the x-ray tube or Jig. A complete description of the vendor commissioning process is described by Wong *et al* (2008) and Tryggestad *et al* (2009). Manufacturer-measured and supplied beam data were compared with all the acquired data during the study.

2.2. Relative dosimetry

2.2.1. Motorized dosimetry system and centralization

All the measurements were performed in a high-resolution 3D scanning water phantom PTW MP3-XS (PTW, Freiburg, Germany) with external dimensions 334 × 336 × 422.5 mm^3 ($L \times W \times H$), which fits inside the SARRP cabinet (figure 1). These dimensions allow us to fulfill the recommendation of the TRS398 for dosimetry of medium energy x-ray, with the phantom dimension extending at least 5 cm beyond all four sides of the largest field size used at the depth of measurement and a margin of at least 10 g cm^{-2} beyond the maximum depth of measurement (IAEA 2000), ensuring full backscatter conditions during characterizations (Chen *et al* 2019). The moving mechanism allows 0.1 mm position reproducibility and a 0.1 mm minimum step size for data acquisition; all the data were collected and visualized by MEPHYSTO mcc software (PTW, Freiburg, Germany). The following radiation dosimeters were used for the relative dosimetry: PTW Diode E (Type 60017) unshielded Diode, a PTW PinPoint 3D-31016 ionization chamber, a PTW 31010 Semiflex ionization chamber and a PTW 34045 Advanced Markus parallel plate ionization chamber. The physical descriptions of each detector from manufacturer specifications are listed in table 1. The ionization chambers were polarized to their respective nominal voltages of +400 V, as indicated by the calibration certificate. Diode E works in photovoltaic mode and was set at 0 V.

As recommended by TRS483 (IAEA 2017) and IPEM 103 (2010), centralization of detectors was performed by measuring in-plane and cross-plane profiles for the 10 × 10 mm^2 small-field size with a fixed collimator at two depths (20 mm and 50 mm) and determining the center point on each in-plane and cross-plane profile. Using this method and software tools, the angle between the scan arm plus detector and beam incidence, as well as the vertical movement and centralization (CAX-central axis deviation), were corrected and adjusted. Then, four profiles with the 10 × 10 mm^2 cone were taken with all the detectors at surface, 5 mm, 20 mm, and 50 mm depth to validate the beam-detector alignment. With the same setup, different profiles were taken for all the detectors and 20 × 20 mm^2 and 40 × 40 mm^2 field sizes for MVC to validate the alignment process with a change

Table 1. Physical characteristics of detectors used in this study.

Ionization chambers			
Detector type	Dimensions of sensitive volume [mm]	Wall material	Central electrode material
PTW 31010 semiflex	Radius 2.75; length 6.5 Volume 0.125 cm^3	Graphite 0.09 mm; PMMA 0.57 mm	Aluminum 99.98; Diameter 1.1 mm
PTW 31016 PinPoint 3D	Radius 1.45; length 2.9 Volume 0.016 cm^3	Graphite 0.09 mm; PMMA 0.57 mm	Aluminum 99.98; Diameter 0.3 mm
PTW 34045 advanced markus	Radius 2.5; depth 1 Volume 0.02 cm^3	0.03 mm PE (Polyethylene)	PMMA, graphite-coated, diameter 5 mm
Solid-state detector			
Detector type	Dimensions of sensitive volume [mm]	Detector material	Shielding
PTW 60017 dosimetry Diode E	Radius 0.56; 30 μm thick Volume 0.03 mm^3	p-type silicon	Not

in wwdetectors and collimator system. As a consequence of the differences between the position of the MVC and the cones at the gantry, verification of the centralization of the detectors must be made for each change in the collimator through the acquisition of multiple profiles at different depths.

2.2.2. Percentage depth dose curves (PDD)

For the 220 kVp, percentage depth ionization curves along the beam central axis were measured for depths between 0 and 80 mm, with all the detectors available described in table 1, for the $40 \times 40\,mm^2$, $20 \times 20\,mm^2$, and $10 \times 10\,mm^2$ field sizes. Cylindrical ionization chambers were positioned with the long axis perpendicular to the direction of the beam. The solid-state detector was positioned with the long axis parallel to the beam. The distance between the source and the water surface (SSD) was placed at 33 cm with the gantry and collimator equal to 0°. Positioning for relative dosimetry was as follows: for the ionization chambers, the measuring point was placed at the center of the sensitive volume of the detector. For Diode E, the reference point was on the axis, 1.33 mm from the detector tip, and for the Advanced Markus parallel plate ionization chamber, it was in the chamber center, 1.3 mm below the surface of the protection cap, according to the technical specifications. Points of measurement for the depth ionization curves were configured according to the measurement regions (buildup or exponential decay region), optimizing the resolution of the steps along the vertical scanning depths: from 0 to 10 mm depth, the scanning step was 0.2 mm; from 10 to 50 mm depth, the step was set to 1 mm; and from 50 to 80 mm depth, the scanning step was 2 mm. The EBT3-Jig PDD curves obtained from the manufacturer are composed of only nine points, corresponding to positioning each film in the middle of the water phantom slabs of 1 cm for the SSD placed at 33 cm in an axial position related to the beam. For evaluation of the EBT3-Jig data, the nine points were exponentially adjusted.

For the ionization chambers, the depth doses were taken to be directly proportional to the readings of the depth ionization without applying any correction factors. Direct depth dose measurements have been reported in similar studies with ionization chambers (Seuntjens and Verhaegen 1996, Knight and Nahum 1994, Hill *et al* 2009, 2014). For Diode E, depth ionization curves were also analyzed without applying any correction factors. It has been reported that PDD measurements with diodes require several correction factors, limiting the direct acquisition of the dose if the correction factors are not accurately known (Ma *et al* 1998). In this work, all the depth ionization curves were named PDD, considering the absence of corrections for Diode E.

All PDD curves were normalized to the dose at 10 mm depth. PDD curves obtained with each detector were compared to the curve measured with the Advanced Markus parallel plate chamber as a reference (Beatty *et al* 1996, Yanch and Harte 1996, Yasuda *et al* 1998, Hill *et al* 2014, Damodar *et al* 2018), and the differences were expressed in terms of the local DD as follows:

$$DD\,(z)\,[\%] = \frac{D_{ref}(z) - D(z)}{D_{ref}(z)} \times 100 \tag{1}$$

where D_{ref} is the dose for the Advanced Markus at z depth, and D is the dose for the detector being evaluated and at the same depth. The global dose differences were also calculated by substituting the term $D_{ref}(z)$ in the denominator of equation (1) by the maximum dose D_{max}, measured with the Advanced Markus for each field size over the full range of depths. The suitability of a parallel plate ionization chamber for PDD measurements, including in regions close to the water surface for x-ray photon beams in the kilovoltage energy range, has been studied in several works (Hill *et al* 2009, 2014).

To determine the suitability of the Advanced Markus ionization chamber as a reference for depth dose curves in small fields, we followed the recommendation of the TRS483 (IAEA 2017), where the minimum field size FWHM, which could be measured with the detector for a given beam quality, to avoid loss of LCPE (lateral charged particle equilibrium range) on the beam axis was calculated as follows:

$$\text{FWHM} \geqslant (2 \times r_{\text{LCPE}}) + d \tag{2}$$

where d is the diameter of the sensitive volume of the detector facing the beam. For the Advanced Markus IC, this value is equal to 5 mm. The range r_{LCPE} is the minimum radius of a circular field for which the collision kerma in water is equal to the absorbed dose in the center of the beam. This range is a parameter used for establishing the relation between the field size and the detector size for which lateral charged particle equilibrium range (LCPE) conditions exist (Attix 1986, IAEA 2017). To estimate the r_{LCPE} range, the mean energy transferred to an electron from a photon in water and the corresponding range for the electron were taken into account. From Johns and Cunningham (1983), a value of r_{LCPE} equal to 0.04 mm was estimated for our beam quality. Then, according to equation (2), a value of FWHM $\geqslant$ 5.1 mm was obtained for maintaining the LCPE conditions. The Advanced Markus chamber was used as the reference for all PDDs at this kVp for field sizes bigger than $10 \times 10\,mm^2$.

Additionally, to estimate the volume averaging effect on our parallel plane detector, the volume averaging correction factor was calculated according to the TRS483 as a 2D integration of the lateral beam profile over the

sensitive area of the detector facing the beam (Laub and Wong 2003, Kawachi *et al* 2008, IAEA 2017). The profiles for the $10 \times 10\,mm^2$ field size, acquired with the high-resolution Diode E at the surface and 5 mm, 20 mm, and 50 mm depths were used for the calculation.

2.2.3. Profile curves

Cross-profile curves were measured with all cylindrical ionization chambers and Diode E for all field sizes, $40 \times 40\,mm^2$, $20 \times 20\,mm^2$, $10 \times 10\,mm^2$, and $5 \times 5\,mm^2$. Cylindrical ionization chambers were positioned with the long axis perpendicular to the direction of the beam and profiles were acquired scanning in the direction of the smaller dimension of the sensitive volume. The solid-state detector was positioned with the long axis parallel to the beam. The SSD was placed to 33 cm with a gantry and collimator equal to 0°, and detectors were all placed at a 20 mm depth. Points of measurement for the profile curves were configured by optimizing the resolution of scanning across the profile by three different regions, the penumbra, flat zone, and outfield region; the penumbra region was set with the maximum resolution. For each scanned field size, the resolution and position-step range were adjusted accordingly; the penumbra and the flat region of the profiles were scanned at a 0.2 mm step size, while the outfield regions were acquired with a 1 mm step size. All profile curves were normalized to the central axis value as 100%. A monitoring ionization chamber was not placed within the beam due to geometrical limitations of the space under the collimators and to avoid perturbations for the smallest field sizes to be measured. To reduce the effects of the dose rate variations in the unit output, an integration time of 0.5 s was applied for the readings with the ionization chambers at each point for the profiles and PDDs. Among the detectors, Diode E has a better response and requires less integration time (PTW Freiburg 2018); therefore, the integration time was set to 0.4 s. The uncertainty due to the missing reference chamber was taken into account.

Different parameters of the profiles were analyzed for all field sizes using software tools and based on the following criteria: the left and right penumbra are calculated as the distance between two dose points (80% and 20% expressed as a percentage of the central axis dose) at the corresponding field boundary. The radiological field size is calculated as the distance between the 50% dose points referred to as the central axis dose (FWHM) on the left and the right side of the beam profile. The profile symmetry was determined within the flattened region as the ratio between the integral over the left half of the profile and the integral over the right half of the profile, calculated from the central axis to the 50% field dose.

Profile curves obtained with each detector and at each field size were compared to the curve measured with the EBT3-Jig (defined as the reference in the analyses); differences were evaluated in terms of the gamma index criterion. The EBT3 radiochromic film detector was defined as the reference because the higher spatial resolution (Azam *et al* 1998).

The budget of expanded uncertainties for the depth ionization curves and profile measurements was estimated by applying the methodology from the ISO guide (1995). The uncertainties from our measurement setup, the detector positioning, the 3D scan system movement, the collimators, the dose rate variations in the output of the x-ray unit, the variation in the mass-energy absorption coefficient of water to air at different depths in the water phantom for the ionization chambers, and the variation of the overall correction factors for the ionization chambers with depth were taken into account in the calculations. The calculated values correspond to a 95.45% confidence level. The uncertainty analysis is presented in table 2.

2.3. Gamma index analyses

A 1D dose distribution gamma index analysis was performed based on the DD and DTA. Evaluated points with $\gamma > 1$ correspond to locations that do not meet the acceptance criteria (Low *et al* 1998). The γ index for profiles was obtained with the *Compare Curves* tool from MEPHYSTO mcc. The criterion of the evaluation was set as 1 mm (DTA)-5% (DD); here, the dose denominator for gamma calculations is the percent value of the maximum measurement point (global maximum dose). Different acceptance criteria in radiotherapy have been analyzed and evaluated by various authors (Stojadinovic *et al* 2015). Considering the challenge in small-field dosimetry with the alignment of beam arm and beam axes, the most rigorous acceptance criteria of 1 mm for DTA were chosen, allowing 5% for DD considering the difference in performance of dose distribution related to the geometrical region in profiles (outfield region, penumbra and plateau) (Fraass *et al* 1998, Stojadinovic *et al* 2015). The gamma index (γ) factor for the entire profile is shown for each field size and detector, compared with the data provided by Xstrahl (EBT3-Jig) as a reference.

For all field sizes and all detectors, the percentage of points with $\gamma \leqslant 1$ for criterion 1 mm–5%, corresponding to the percentage of locations where the evaluated point does not meet the acceptance criteria, is presented. The impacts of various acceptance criteria were evaluated for a $20 \times 20\,mm^2$ profile and all detectors. In our case, the gamma index allows an integral evaluation of the orientation of the beam related to the dosimetric set, physical symmetry of collimators, and CAX alignment of the arm related to the beam. CAX has been analyzed to discard

Table 2. Estimated uncertainties associated with the experimentally measured depth dose data and profiles using the ISO methodology.

Depth dose data	Type A(%)	Type B(%)
Repeatability of the measurements	0.11	
Setting of the zero position of the detector		0.07
SSD setting		0.15
Accuracy of the water tank motors for positioning		0.07
Variation of (μ/ρ) with depth for the ionization chambers		1.00
Variation of the overall correction factor k_{ch} with depth		1.00
Dose rate variations in x-ray unit output		0.11
Drift of the measuring equipment		0.30
Expanded uncertainty	2.90% ($k = 2$)	
Profile data	**Type A(%)**	**Type B(%)**
Repeatability of the measurements	0.11	
Setting of the zero position of the detector		0.58
SSD setting		0.15
Accuracy of the water tank motors for positioning		0.58
Variation in the angular response of the chambers		0.80
Dose rate variations in x-ray unit output		0.11
Drift of the measuring equipment		0.30
Expanded uncertainty	2.40% ($k = 2$)	

major variations due to misalignment. The extra acceptance criteria evaluated were 2 mm/5%, 1 mm/2% and 3 mm/3%, which is widely used in clinical dosimetry (Stojadinovic *et al* 2015).

3. Results and discussion

3.1. Positioning and centralization method

Figure 2(a) shows the final four profiles with the Diode E detector at the surface and at 5 mm, 20 mm, and 50 mm depths, after than the angulations of the scan arm relative to the beam were corrected. Figure 2(b) shows the final central axis deviation (CAX) of the profiles with all the detectors and the EBT3-Jig for the surface and 5 mm, 20 mm, and 50 mm depths for the 10 × 10 mm^2 cone. The maximum CAX deviation is 0.12 mm at a 50 mm depth. The maximum CAX deviation reported by the software for the 40 × 40 mm^2 and 20 × 20 mm^2 field sizes is better than 0.1 mm. Some readjustments were necessary as a consequence of the differences between the central physical position of the MVC and the cones (approximately 1.7 mm).

According to the error estimated for other studies, due to misalignment of the system for small-field dosimetry, alignment better than 1 mm must be achieved for the smallest field size (IPEM 2010). In SARRP, considering that for a 5 × 5 mm^2 cone, a misalignment of 1 mm represents 20% of the field size, an extremely rigorous centralization must be performed. The use of the scanning system and the two profiles method for alignment as suggested for protocols (IPEM 2010, IAEA 2017) led to a maximum CAX deviation better than 0.1 mm for our measurements. With the use of a 3D scanning system, it is possible to make a radiological adjustment of the position of the detectors. This procedure is fundamental to properly measuring field sizes of millimeter dimensions with adequate centralization that is maintained in depth.

3.2. Depth dose curves

The expanded uncertainty in the measured depth dose data was calculated to be 2.9% ($k = 2$) at the 95.45% confidence level. The following results present the measured data with the ionization chambers and the solid-state detector without the application of any correction factors, and the depth dose provided by the manufacturer measured with EBT3 for all 40 × 40 mm^2, 20 × 20 mm^2, and 10 × 10 mm^2 field sizes. The volume averaging effect factor for the Advanced Markus parallel plate and the 10 × 10 mm^2 cone, calculated in accordance with the TRS483, gave a value of 1 for the profiles at the surface and at 5 mm and 20 mm depths. Considering that 10 mm is the diameter of the smallest field size in our study, the depth ionization curves were not corrected for the volume effect.

Figures 3(a) and 4(a) show the depth dose curves for 40 × 40 mm^2 and 20 × 20 mm^2, all the ionization chambers exhibit very good agreement with the reference. For the PinPoint 3D, the global dose difference is better than 1% even at the surface; for the Semiflex 31010, it is better than 1.2% for measurements deeper than 5 mm, and for Diode E, it is near 3.5%. For EBT3-Jig, the maximum global dose difference is 2%. Figures 3(b) and 4(b) show the local dose differences for 40 × 40 mm^2 and 20 × 20 mm^2, respectively, between the curves with the Semiflex

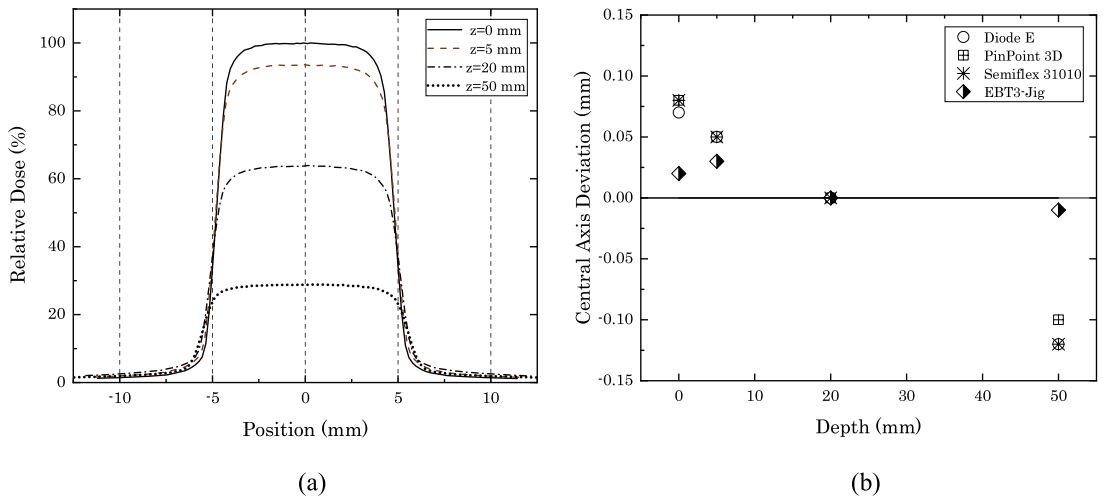

Figure 2. (a) Profiles for a 10 × 10 mm^2 cone with Diode E detector at different depths. (b) Central axis deviation of 10 × 10 mm^2 cone profiles for different detectors and depths.

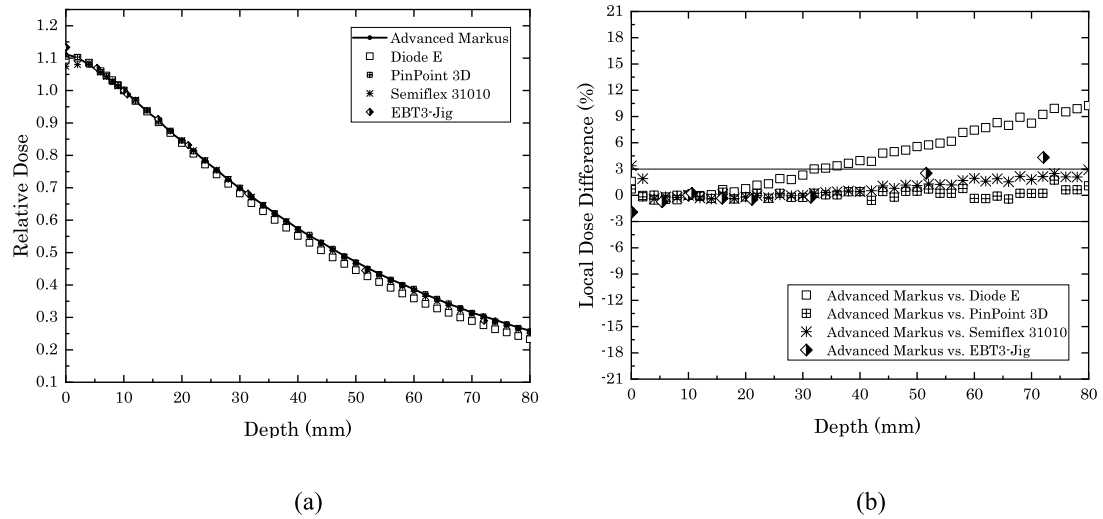

Figure 3. For SARRP 40 × 40 mm^2. (a) Measured percentage depth dose curves for three ionization chambers, a solid-state detector and EBT3 film. (b) PDD local dose difference between the detectors and the parallel plate ionization chamber.

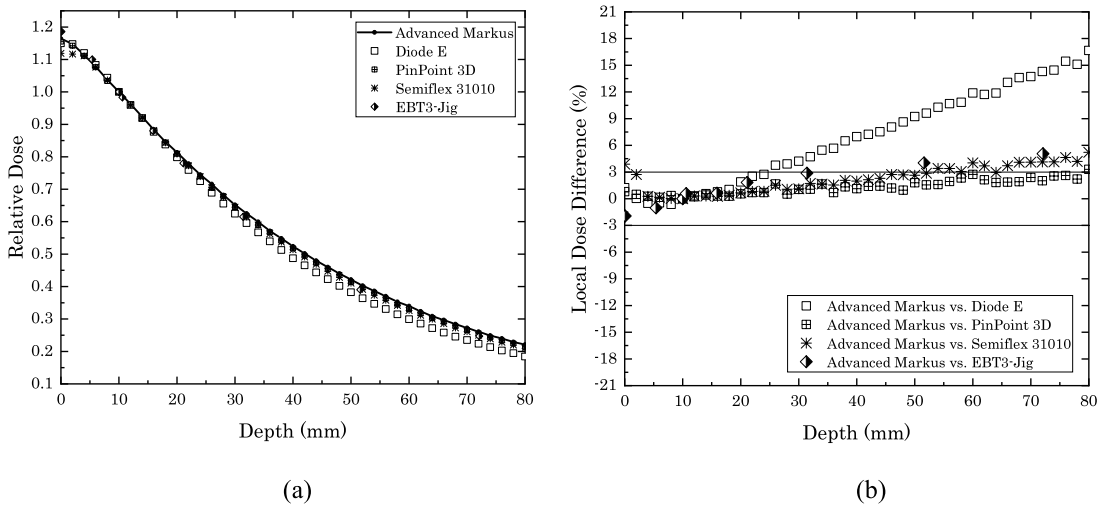

Figure 4. SARRP 20 × 20 mm^2. (a) Measured percentage depth dose curves for three ionization chambers, a solid-state detector and EBT3 film. (b) PDD local dose difference between detectors and the parallel plate ionization chamber.

31010 small-chamber, the PinPoint 3D microchamber, the Diode E and the EBT3-Jig compared to the curve for the Advanced Markus parallel plate. Evaluation of the local dose difference allows visualization of the behavior of the curves in the different regions (buildup and exponential attenuation). For the PinPoint 3D microchamber, the agreement is very good for both field sizes, better than 2% for the first 50 mm and increasing up to 3.3% with depth for the $20 \times 20\,mm^2$ field size. For the Semiflex 31010 small-chamber, the agreement with the reference is better than 3% for both field sizes for the first 50 mm and increases up to 5% at the last depths for the $20 \times 20\,mm^2$ field size. For the first 5 mm, the small chamber exhibits local differences of approximately 4%.

The results with the ionization chambers are consistent with similar measurements from a previous study (Hill *et al* 2009, Damodar *et al* 2018). For Semiflex 31010, there is a dose artifact at the first 5 mm. This artifact could be explained by the detector partly being irradiated out of the water as it moves to the surface. As this effect depends on the volume of the detector, it probably leads to doses lower than 0.7% for the PinPoint 3D and 4% for the Semiflex 31010. The volume average due to the sizes of the cylindrical ionization chambers related to field sizes and dose gradients is consistent with similar measurements from previous studies (Hill *et al* 2009). Very good performance has been reported for the Semiflex 31010 in terms of stability in a 220 kVp x-ray unit (Kuess *et al* 2014). The Diode E detector shows the most dramatic local difference, with considerable under-response compared with the reference, with local dose differences near 5% for the first 50 mm but increasing up to 10% and 16% with depth for the $40 \times 40\,mm^2$ and $20 \times 20\,mm^2$ field sizes, respectively. Unlike the results reported by Damodar *et al* (2018) for a beam of 280 kVp and much larger field sizes, in our study, compared with the ionization chambers, the Diode presents an under-response in the readings for fields equal to or less than $40 \times 40\,mm^2$. The higher physical density of the silicon related to water may produce this larger change in the response compared with that of thimble ionization chambers (Scott *et al* 2012), influenced by the fast drop in dose for this energy with the spectral changes with depth. The EBT3 film coupled to the Jig system shows local differences in depth dose increasing up to 5% with increasing depth.

Figure 5(a) shows the depth dose curves for $10 \times 10\,mm^2$. For the PinPoint 3D, the maximum global dose difference is better than 1% over the full range of depths, for the Semiflex 31010 it is better than 1.5% and for EBT3-JIG it is better than 2%. For the first 5 mm, the small-chamber exhibits a global difference of 3%. For Diode E, the maximum global difference is 4.5%, reaching this value at the lowest depths.

Figure 5(b) shows the local dose difference between detectors and parallel plate chambers. For this field size, the PinPoint 3D microchamber has good agreement with the reference better than 2% from the surface until 50 mm depth, showing differences increasing up to 4.5% for the last depths points. The Semiflex 31010 chamber shows differences near 4% until 50 mm depth, increasing up to 6.5% at the last millimeters. The EBT3 film coupled to the Jig system shows differences in depth dose increasing up to 10%.

The Diode E detector shows the higher local difference compared to the Advanced Markus, with a difference increasing up to 21% with depth compared with the larger field sizes. When the field size decreased and the number of low-energy photons decreased, the mean energy of the photon spectrum increased and the ratio of mass energy absorption coefficient $\left(\frac{\mu_{en}}{\rho}\right)_{Si}^{water}$ decreased. The influence of low-energy scattered photons increases with depth and the lack of water equivalence (IPEM 2010). The progressive increase in the local dose difference of the Diode compared to the reference when it decreases to $10 \times 10\,mm^2$ suggests a high dependence of the detector response on the field size, in consequence the Diode E should not be recommended for the acquisition of PDD curves for photon fields in a 220 kVp beam when correction factors are not accurately known, in agreement with the similar results of the study developed by Damodar *et al* (2018) for 280 kVp x-ray beams for non-small photon fields.

The variations in the response between the Advanced Markus IC assembled with a graphite electrode and the thimble-type ionization chambers assembled with aluminum electrodes could be explained by differences in the material of the central electrode. In agreement with the study of Muir and Rogers (2011), the differences between the cylindrical ionization chambers could be explained by the larger fraction of the collecting volume occupied by the electrode of the Semiflex 31010 CI compared to the PinPoint 3D IC. For ionization chambers where the electrode is composed of the same material as the wall, as the Advanced Markus IC, variations in the response resulting from the effect of the central electrode are negligible. All PDD curves measured with the cylindrical ionization chambers showed better agreement with the reference curve than the manufacturer data. Differences between the manufacturer's dosimetry and the user's dosimetry for this system as well as the effect of different setups (axial or longitudinal) for EBT3 film dosimetry, mainly for the PDDs, have also been reported by other authors (Wang *et al* 2018).

3.3. Profile curves

The expanded uncertainty in the measured profile data was calculated to be 2.4% ($k = 2$) at the 95.45% confidence level. The following results present the measured data with the ionization chambers and the solid-state detector compared with the profiles measured with the manufacturer system based on radiochromic film,

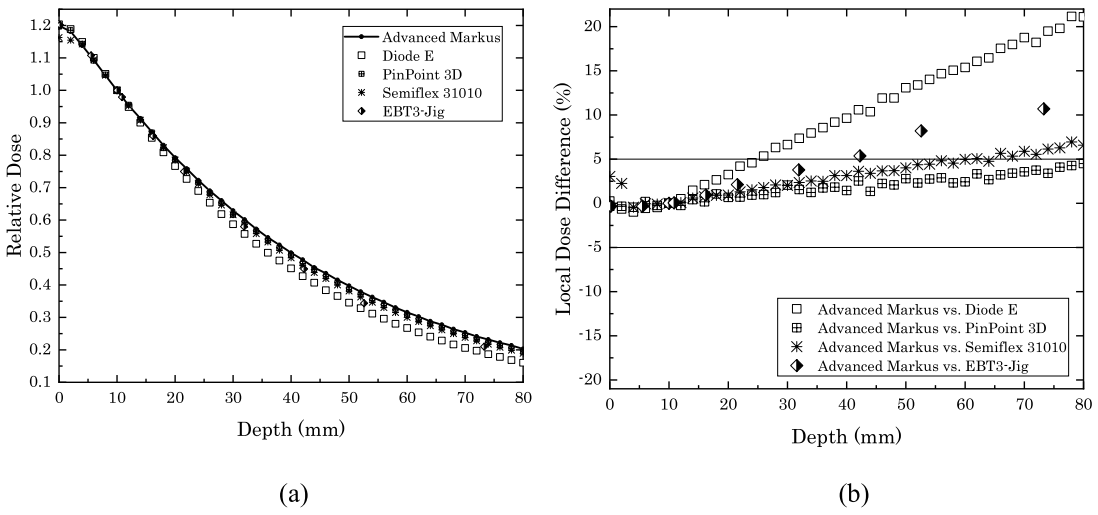

Figure 5. For SARRP 10 × 10 mm^2. (a) Measured percentage depth dose curves for three ionization chambers, a solid-state detector and EBT3 film. (b) PDD local dose difference between detectors and the parallel plate ionization chamber.

Table 3. Penumbra left and right, radiological field size expressed as FWHM and symmetry from profiles at SSD = 33 cm and depth 2 cm for different detectors and field sizes for SARRP.

40 × 40 mm^2	Penumbra left [mm]	Penumbra right [mm]	Radiological field size (FWHM) [mm]	Symmetry [%]
Semiflex 31010	4.36	4.36	39.03	0
PinPoint 3D	2.56	2.69	38.89	0.16
Diode E	2.53	2.57	38.71	0.24
Jig-EBT3	1.75	1.76	38.81	0.22
20 × 20 mm^2				
Semiflex 31010	3.35	3.35	19.17	0
PinPoint 3D	2.03	2.03	18.93	0.19
Diode E	1.74	1.74	18.90	0
Jig-EBT3	1.03	0.97	18.61	0.1
10 × 10 mm^2				
Semiflex 31010	2.86	2.86	10.29	0.02
PinPoint 3D	1.68	1.76	10.27	0.58
Diode E	0.94	0.98	10.22	0.20
Jig-EBT3	0.40	0.41	10.20	0.19
5 × 5 mm^2				
PinPoint 3D	1.53	1.53	5.27	0.50
Diode E	0.81	0.81	5.21	0.06
Jig-EBT3	0.37	0.38	5.16	0.10

the gamma index analyses across all profiles for criterion 1 mm–5% are also shown. The measured values of the penumbra, radiological field size and symmetry are tabulated in table 3.

Figures 6(a) and (c) show the profile curves for the 40 × 40 mm^2 and 20 × 20 mm^2 for all detectors. Very good agreement was found among Diode E, PinPoint 3D, and EBT3-Jig. A smaller off-axis perturbation factor, as well as a uniform directional response for high-energy small photon fields, was previously reported for the PinPoint 3D ionization chambers (Scott *et al* 2012). We obtained a similar response for the kV photon beams in our study. The symmetry values related to the final CAX alignments are better than 0.24%. Differences in the penumbra are better than 0.81 mm between Diode E and EBT3-Jig and 1.1 mm between PinPoint 3D and EBT3-Jig. The Semiflex 31010 ionization chamber shows the maximum difference in the penumbra of 2.6 mm, and the difference in FWHM is 0.5 mm larger than recorded with EBT3-Jig, which may be attributed to the dose averaging effect across the finite volume of a detector, leading to penumbra broadening (IAEA 2000, Scott *et al* 2012, IAEA 2017).

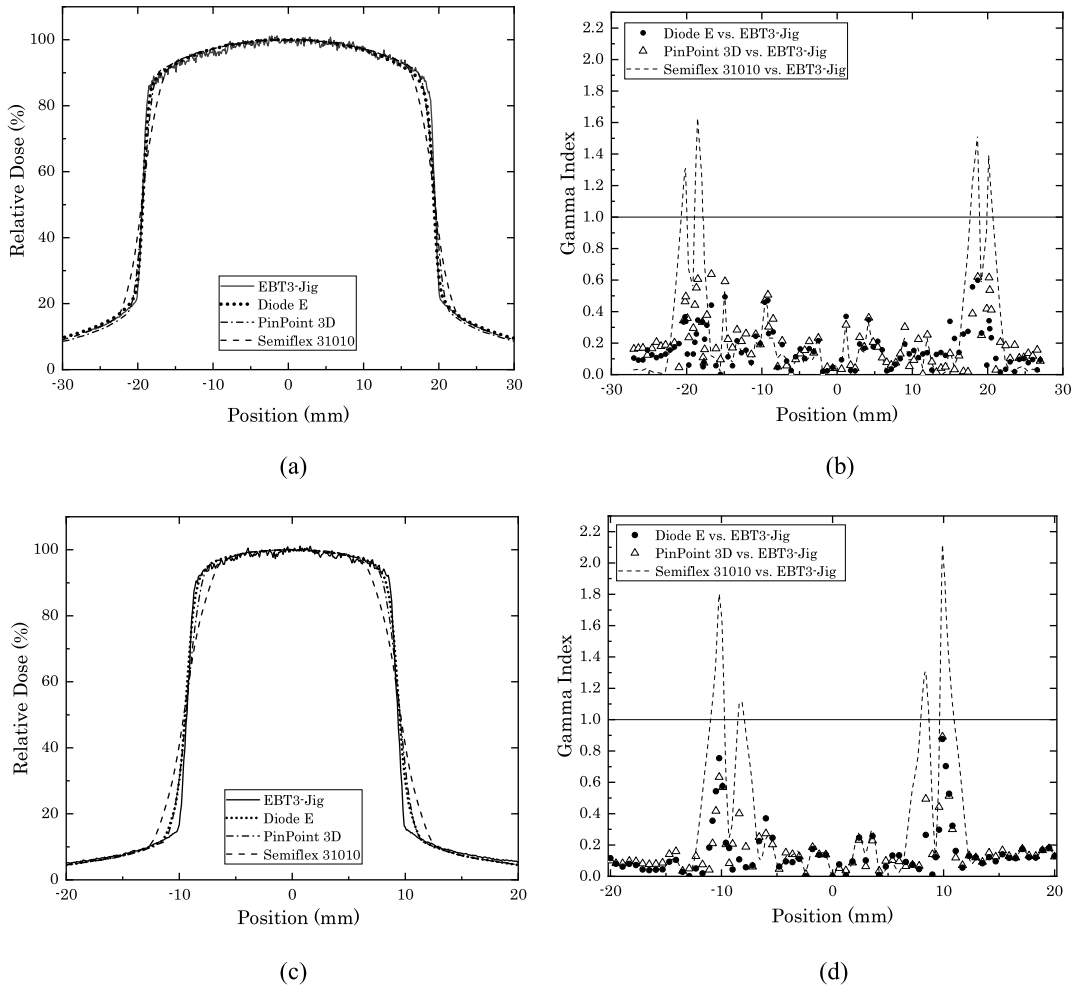

Figure 6. Measured profile curves for two ionization chambers, a solid-state detector, and EBT3, SSD = 33 cm and $z = 20$ mm. (a) MVC 40 × 40 mm^2. (c) MVC 20 × 20 mm^2. Gamma index γ (1 mm–5%) for two ionization chambers and a solid-state detector profiles compared to the EBT3-Jig profile as a reference. (b) 40 × 40 mm^2. (d) 20 × 20 mm^2.

Figure 6(b) shows the gamma index for 40 × 40 mm^2 for the PinPoint 3D microchamber, Diode E and Semiflex 31010 small-chamber, compared to the EBT3-Jig as a reference. For Diode E and PinPoint 3D, the maximum γ is 0.65, with 99% of the points showing a $\gamma < 0.6$. For the Semiflex 31010, the γ value reaches a maximum of 1.62, with 93% of the points showing a $\gamma < 1$; however, 7% of the points that do not meet the gamma criteria correspond to the penumbra zone. For the Semiflex 31010, the penumbra corresponds to approximately 11% of the radiation field, compared to 4% for EBT3. A careful analysis should be made of the types of treatment that will be carried out with the micro irradiator if this type of detector is used in the commissioning of this field size.

Figure 6(d) shows the gamma index for 20 × 20 mm^2 for the PinPoint 3D, Diode E and Semiflex 31010, compared to EBT3-Jig. For Diode E and PinPoint 3D, the maximum γ is 0.9, with 98% of the points showing a $\gamma < 0.6$. For the Semiflex 31010 γ, the value reaches a maximum of 2.1, with 90% of the points showing a $\gamma < 1$; however, the value of penumbra is very compromised. For this reason, the Semiflex 31010 should not be recommended for the measurement of profiles with sizes equal to or smaller than 20 × 20 mm^2 at this beam energy.

Figure 7(a) shows the profile curves for the 10 × 10 mm^2 cone with all detectors. For the PinPoint 3D and Diode E, the agreement is very good compared to EBT3-Jig, even for the 80%–20% penumbra, where it is possible to visualize a larger effect of volume averaging when the field size is smaller; the same effect occurs in the in-plane and cross-plane directions of the beam, contributing to a larger effect in thimble chambers with differences between the length and the diameter. Differences in the penumbra are better than 0.6 mm and 1.4 mm for Diode E and PinPoint 3D detectors. Symmetry values are better than 0.6%. For the Semiflex 31010 ionization chamber, as a consequence of the volume averaging effect, the difference in the penumbra is 2.5 mm. Radiological field sizes expressed as FWHM are very similar for all detectors.

Figure 7(b) shows the gamma index for the PinPoint 3D, Diode E and Semiflex 31010. For Diode E, the profile is in very good agreement with the reference. For Diode E and PinPoint 3D detectors, 100% of the points show a $\gamma < 1$, with maximum values of 0.56 and 0.95, respectively. If PinPoint 3D is chosen to measure this field size, special attention should be paid for very conformal planning because of the penumbra value due to volume aver-

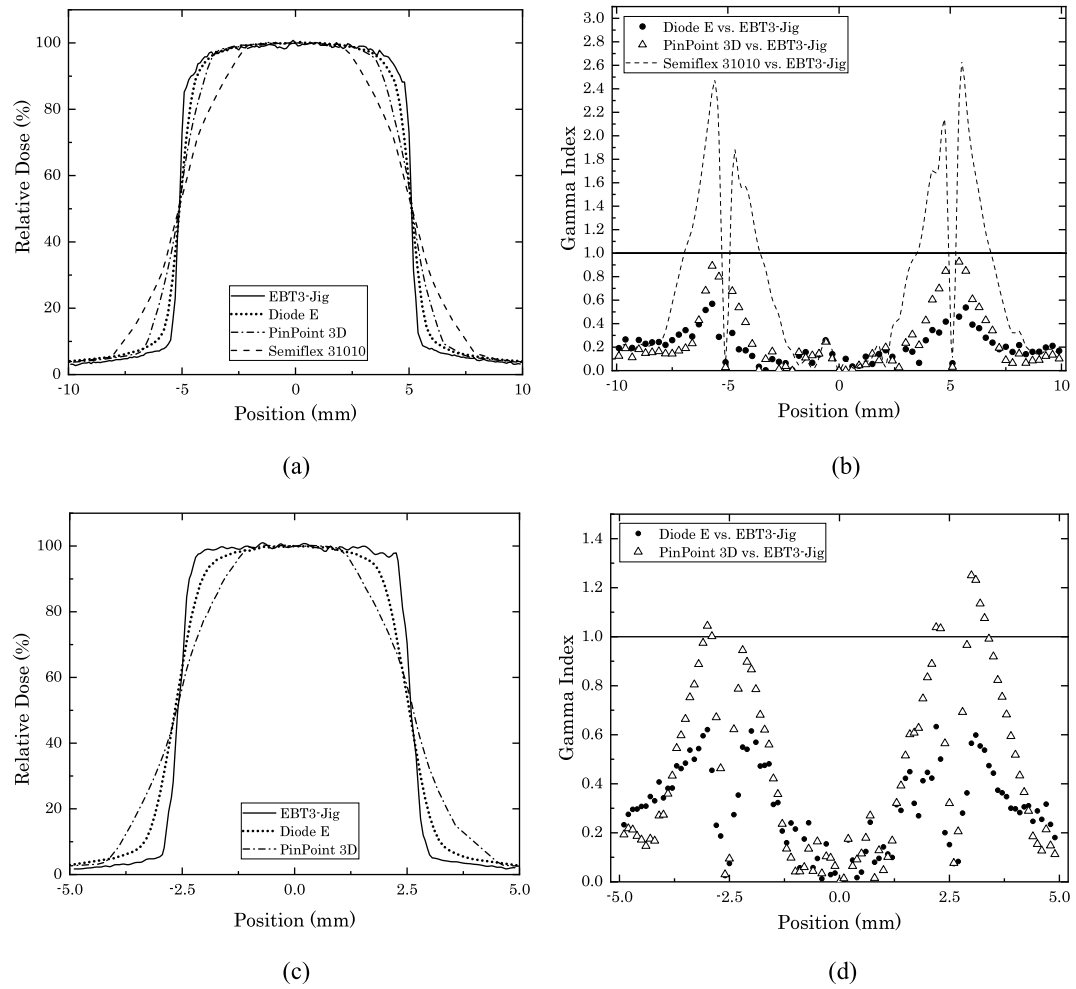

Figure 7. Measured profile curves for one ionization chamber, a solid-state detector, and EBT3; SSD = 33 cm and $z = 20$ mm. (a) $10 \times 10\,mm^2$. (c) $5 \times 5\,mm^2$. Gamma index γ (1 mm–5%) for one ionization chamber and a solid-state detector profiles compared to the EBT3-Jig profile as a reference. (b) $10 \times 10\,mm^2$. (d) $5 \times 5\,mm^2$.

aging. For Semiflex 31010, almost 32% of the points have a $\gamma > 1$, where the maximum value is 2.4, indicating that this detector is not suitable for measuring this field size.

Figure 7(c) shows profile curves for the cone of $5 \times 5\,mm^2$ with the PinPoint 3D, Diode E and EBT3-Jig. For Diode E, the agreement is very good compared to the EBT3-Jig, even for the 80%–20% penumbra where the difference in the penumbra is 0.44 mm, in agreement with previous findings evaluating the FWHM for small field sizes for high-energy photon beams (Scott *et al* 2012). For the PinPoint 3D detector, the difference in the penumbra is better than 1.2 mm. Symmetry values are better than 0.5%. Figure 7(d) shows the gamma index for PinPoint 3D and Diode E. The profile for Diode E is in very good agreement with the reference, with a $\gamma < 0.61$ for 100% of the points. The profile for PinPoint 3D is in good agreement with $\gamma < 1$ for 93% of the points; however, the penumbra value is a high percentage of the radiological field size. Values of $\gamma > 1$ are in the penumbra area and are due to the average volume effect of this detector for the smaller field size of $5 \times 5\,mm^2$. In this case, only the Diode E detector could be recommended for this small field size.

3.4. Gamma index analyses

In figure 8(a), the percentage of points with γ lower than 1 for the criteria 1 mm–5% is presented for all detectors compared to the manufacturer data with EBT3-Jig. Profiles for all field sizes were analyzed. Diode E and PinPoint 3D detectors have good agreement for all field sizes greater than or equal to $10 \times 10\,mm^2$, with 100% of points with $\gamma < 1$. For the $5 \times 5\,mm^2$ Diode E detector, the best performance was observed. Profiles with Semiflex 31010 have a good agreement for $40 \times 40\,mm^2$ field size; however, as a consequence of the sharper penumbra for this beam, the value of the penumbra is a criterion of decision and choice of the detector, leading to the question of whether highly conformed studies will be carried out with the irradiator, leading to a rationale for decreasing the margins of the target.

The penumbra is an important part of treatment planning considerations, especially for conformal and stereotactic situations. The use of the PTV (planning target volume) as a geometric margin for hypofractionated

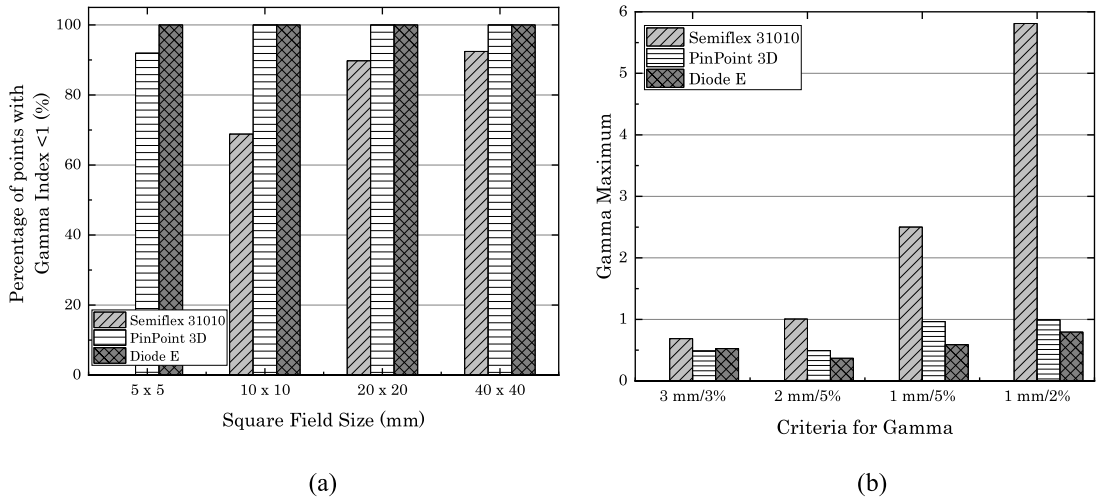

Figure 8. (a) Percentage of points with gamma index <1, criteria 1 mm/5%, for all field size profiles, between all detectors and EBT3-Jig. (b) Maximum gamma index for 10 × 10 mm^2 profiles, for different criteria, between all detectors and EBT3-Jig SSD = 33 cm z = 20 mm.

and highly shaped irradiations is a topic of current discussion (ICRU 2017). Following international recommendations (ICRU 1999), the penumbra is considered an extra margin that must be added to the PTV; however, if it is not used, the irradiation could be delivered onto a smaller volume that considers only the main target. If irradiation is intended following this approach, a detector with the smallest possible sensitive volume should be chosen during the commissioning of the beam to have a very precise characterization of the penumbra and avoid large dose variations in the volume of interest. If only a detector with a large sensitive volume is available, the use of additional margins during irradiation should be considered to avoid large dose variations at the periphery of the main target.

With regard to planning considerations, in a study of small MV field profiles that evaluated the differences in the FWHM for a solid-state detector and a PinPoint ionization chamber compared to Monte Carlo calculations, the same FWHM value has been reported for the solid-state detector and the MC profile, and differences near 6% have been reported between the PinPoint IC and the MC profile for a 5 mm square field in water. That study, also reported that the integral doses for small fields (integral areas under the field profiles multiplied by their corresponding output factors) for volumetric modulated arc therapy (VMAT) or intensity modulated radiotherapy (IMRT) plans, composed of many overlapping small fields, would be approximately correct for both detectors (Scott *et al* 2012). Given the results of this study, it would be necessary to evaluate the behavior of plans with multiple conformed small fields in the kV energetic range, and gamma index analyses could facilitate this assessment.

In figure 8(b), several gamma index criteria were tested to evaluate the γ Index sensitivity. For the 10 × 10 mm^2 fixed cone, the criteria evaluated were 2 mm/5%, 1 mm/5%, 1 mm/2% DTA/DD and the regular clinical standard quality assurance criteria 3 mm/3%. For the acceptance criteria of 1 mm/2% in this study, a maximum γ value of 5.8 for the Semiflex 31010 ionization chamber was obtained; this γ value would be unacceptable from a clinical point of view (Miften *et al* 2018). For the PinPoint 3D and Diode E detector, this same criterion is passing with 100% of evaluated points with a $\gamma < 1$.

The same analysis can be performed for all other acceptance criteria, and the election of this criteria must consider which of the gamma analysis components would have the greatest impact on the analysis. In our study, we have given special attention to the evaluation of the CAX deviation and field size definition for which we have chosen a very strict (DTA) value (1 mm). For the percentage value (DD), in agreement with the figure, varying the DD value does not have the same impact as varying DTA for those field sizes. In contrast, as suggested by Stojadinovic *et al* (2015), final gamma index criteria can be defined by dividing dose distributions in regions of high dose, low dose, and high dose gradient. This method could allow changing from a global dose assessment to a local evaluation according to the regions of interest. As found in this study, a high dose gradient area represents the highest gamma index values.

4. Conclusions and future perspectives

In this study, we evaluated the performance of a number of detectors, including newer models that have not been systematically investigated for small fields in water, in their suitability for relative dosimetry for a conformal biological micro irradiator SARRP system with kilovoltage x-ray photon beams (220 kVp). The use of a high-resolution 3D scan and the two-profile method for alignment leads to a maximum CAX deviation better than

0.1 mm for our measurements; this value is near, or in some cases better than, that for the manufacturer system. Compared with the Advanced Markus parallel plate ionization chamber for PDD, the Semiflex 31010 (for depth measurements over a depth of 5 mm) and the PinPoint 3D cylindrical ionization chambers exhibited a very good agreement better than 1.5% when the global dose differences were evaluated for all field sizes. All PDD curves measured with cylindrical ionization chambers showed better agreement with the reference curves than the manufacturer data. The unshielded diode detector shows the most dramatic differences exhibiting high field size dependence. For this reason, this detector should not be recommended for the acquisition of PDD curves in a 220 kVp beam if correction factors are not accurately known. In agreement with the gamma index analyses, the PinPoint 3D ionization chamber and Diode E are very good candidates for profile measurements. Only the Diode E detector could be recommended for a $5 \times 5\,mm^2$ profile. Future work will include expanding dosimetry in water with solid-state detectors with better response reported for this energy range as a microdiamond detector (Damodar *et al* 2018, Kampfer *et al* 2018). Considering that current dosimetry is manufacturer dependent and only standardized for the SARRP system, even with good results, it is necessary to obtain independent standardization of the beam characterization, mainly in water-based dosimetry for small fields.

Acknowledgments

This work was partly supported by the fellowship DSC—Proc. Number 200.516/2018 from the Foundation for Research Support of the State of Rio de Janeiro-FAPERJ, Brazil. The authors gratefully acknowledge PTW Latin America for the loan of equipment and detectors to develop this study.

Disclosure of conflicts of interest

The authors do not have conflicts of interest to disclose.

ORCID iDs

Erika Muñoz Arango https://orcid.org/0000-0002-3506-1554

References

Attix F H 1986 *Introduction to Radiological Physics and Radiation Dosimetry* (New York: Wiley)
Azam N-R, Blackwell C, Coursey B, Gall K, Galvin J, McLaughlin W, Meigooni A, Nath R, Rodgers J and Soares C 1998 Radiochromic film dosimetry *AAPM Technical Report* No. 63 (The American Association of Physicists in Medicine)
Bazalova M, Nelson G, Noll J M and Graves E E 2013 Modality comparison for small animal radiotherapy: a simulation study *Med. Phys.* **41** 011710
Beatty J, Biggs P J, Gall K, Okunieff P, Pardo F S, Harte K J, Dalterio M J and SliskiA P 1996 A new miniature x-ray device for interstitial radiosurgery: dosimetry *Med. Phys.* **23** 53–62
Chen Q, Molloy J, Izumi T and Sterpin E 2019 Impact of backscatter material thickness on the depth dose of orthovoltage irradiators for radiobiology research *Phys. Med. Biol.* **64** 055001
Cheng C-W, Hyun Cho S, Taylor M and Das I J 2007 Determination of zero-field size percent depth doses and tissue maximum ratios for stereotactic radiosurgery and IMRT dosimetry: comparison between experimental measurements and Monte Carlo simulation *Med. Phys.* **34** 3149–57
Damodar J, Odgers D, Pope D and Hill R 2018 A study on the suitability of the PTW microDiamond detector for kilovoltage x-ray beam dosimetry *Appl. Radiat. Isot.* **135** 104–9
Desrosiers M, Dewerd L, Deye J, Lindsay P, Murphy M K, Mitch M, Macchiarini F, Stojadinovic S and Stone H 2013 The importance of dosimetry standardization in radiobiology *J. Res. Natl Inst. Stand. Technol.* **118** 403–18
Dos Santos M, Paget V, Ben Kacem M, Trompier F, Benadjaoud M A, François A, Guipaud O, Benderitter M and Milliat F 2018 Importance of dosimetry protocol for cell irradiation on a low x-rays facility and consequences for the biological response *Int. J. Radiat. Biol.* **94** 597–606
Fraass B, Doppke K, Hunt M, Kutcher G, Starkschall G, Stern R and Van Dyke J 1998 AAPM Task Group 53: quality assurance for clinical radiotherapy treatment planning *Med Phys.* **25** 1773–829
Ghita M *et al* 2017 Small field dosimetry for the small animal radiotherapy research platform (SARRP) *Radiat. Oncol.* **12** 1–10
Hill R, Healy B, Holloway L, Kuncic Z, Thwaites D and Baldock C 2014 Advances in kilovoltage x-ray beam dosimetry *Phys. Med. Biol.* **59** 183–231
Hill R, Mo Z, Haque M and Baldock C 2009 An evaluation of ionization chambers for the relative dosimetry of kilovoltage x-ray beams *Med. Phys.* **36** 3971–81
IAEA 2000 Absorbed dose determination in external beam radiotherapy *Technical Report Series* No. 398 International Atomic Energy Agency
IAEA 2017 Dosimetry of small static fields used in external beam radiotherapy an international code of practice for reference and relative dose determination *Technical Report Series No.* 483 International Atomic Energy Agency
ICRU 1999 Prescribing, recording and reporting photon beam therapy (supplement to ICRU report 50) *Technical Report* No. 62 International Commission on Radiation Units and Measurements
ICRU 2017 Prescribing, recording and reporting of stereotactic treatments with small photon beams *Technical Report* No. 91 International Commission on Radiation Units and Measurements

IPEM 2010 Small field MV photon dosimetry *IPEM Report* No. 103 (Institute of Physics and Engineering in Medicine)
ISO 1995 *Guide to the Expression of Uncertainties in Measurement* 2nd edn (International Organisation for Standardization)
Johns H E and Cunningham J R 1983 *Physics of Radiology* 4th edn (Springfield: Charles C Thomas)
Johnstone C D, Therriault-Proulx F, Beaulieu L and Bazalova-Carter M 2018 Characterization of a plastic scintillating detector for the small animal radiation research platform (SARRP) *Med. Phys.* 394–404
Kampfer S, Cho N, Combs S E and Wilkens J J 2018 Dosimetric characterization of a single crystal diamond detector in x-ray beams for preclinical research *Z. Med. Phys.* **28** 303–9
Kawachi T, Saitoh H, Inoue M, Katayose T, Myojoyama A and Hatano K 2008 Reference dosimetry condition and beam quality correction factor for CyberKnife beam *Med. Phys.* **35** 4591–8
Knight R and Nahum A 1994 Depth and field-size dependence of ratios of mass-energy absorption coefficient, water-to-air, for kV x-ray dosimetry *Proc. IAEA Int. Symp. on Measurement Assurance in Dosimetry* vol IAEA-SM-330/17 (Vienna: IAEA) pp 361–70
Kuess P, Bozsaky E, Hopfgartner J, Seifritz G, Dörr W and Georg D 2014 Dosimetric challenges of small animal irradiation with a commercial x-ray unit *Z. Med. Phys.* **24** 363–72
Laub W U and Wong T 2003 The volume effect of detectors in the dosimetry of small fields used in IMRT *Med. Phys.* **30** 341–7
Lindsay P E *et al* 2014 Multi-institutional Dosimetric and geometric commissioning of image-guided small animal irradiators *Med. Phys.* **41** 031714
Liu F-F *et al* 2013 Lessons learned from radiation oncology clinical trials *Clin. Cancer Res.* **19** 6089–100
Low D A, Harms W B, Mutic S and Purdy J A 1998 A technique for the quantitative evaluation of dose distributions *Med. Phys.* **25** 656–61
Ma C-M, Coffey C W, Dewerd L A, Liu C, Nath R, Seltzer S M and Seuntjens J P 2001 AAPM Protocol for 40–300 kV x-ray beam dosimetry in radiotherapy and radiobiology *Med. Phys.* **28** 868–93
Ma C-M, Li X A and Seuntjens J P 1998 Study of dosimetry consistency for kilovoltage x-ray beams *Med. Phys.* **25** 2376–84
Miften M *et al* 2018 Tolerance limits and methodologies for IMRT measurement-based verification QA: recommendations of AAPM Task Group No. 218 *Med. Phys.* **45** e53–83
Mijnheer B 2018 *Clinical 3D Dosimetry in Radiation Therapy* 1st edn, ed L Taylor and Francis Group (Boca Raton, FL: CRC Press)
Muir B R and Rogers D W O 2011 The central electrode correction factor for high-Z electrodes in small ionization chambers *Med. Phys.* **38** 1081–8
Muñoz E, Peixoto J G and de Almeida C E 2019 Uma revisão crítica dos processos de translação EM radioterapia pre-clínica associada às limitações na dosimetria de irradiadores biológicos conformacionais *Braz. J. Radiat. Sci.* **7** 01–18
Na Y H, Wang Y-F, Black P J, Velten C, Qian X, Lin S-C, Adamovics J and Wuu C-S 2018 Dosimetric and geometric characteristics of a small animal image-guided irradiator using 3D dosimetry/optical CT scanner *Med. Phys.* **45** 3330–9
Newton J, Oldham M, Thomas A, Li Y, Adamovics J, Kirsch D G and Das S 2011 Commissioning a small-field biological irradiator using point, 2D, and 3D dosimetry techniques *Med. Phys.* **38** 6754–62
Pidikiti R, Stojadinovic S, Speiser M, Song K H, Hager F, And D S and Solberg T D 2011 Dosimetric characterization of an image-guided stereotactic small animal irradiator *Phys. Med. Biol.* **56** 2585–99
PTW 2018 *Small Field Dosimetry Application Guide When Small Things Matter* (Freiburg: PTW)
Scott A J D, Kumar S, Nahum A E and Fenwick J D 2012 Characterizing the influence of detector density on dosimeter response in non-equilibrium small photon fields *Phys. Med. Biol.* **57** 4461–76
Seuntjens J and Verhaegen F 1996 Dependence of overall correction factor of a cylindrical ionization chamber on field size and depth in medium-energy x-ray beams *Med. Phys.* **23** 1789–96
Stojadinovic S, Ouyang L, Gu X, Pompoš A, Bao Q and Solberg T D 2015 Breaking bad IMRT QA practice *J. Appl. Clin. Med. Phys.* **16** 154–65
Tryggestad E, Armour M, Iordachita I, Verhaegen F and Wong J W 2009 A comprehensive system for dosimetric commissioning and Monte Carlo validation for the small animal radiation research platform *Phys. Med. Biol.* **54** 5341–57
Verhaegen F *et al* 2018 ESTROACROP: Technology for precision small animal radiotherapy research: optimal use and challenges *Radiother. Oncol.* **126** 471–8
Verhaegen F, Granton P and Tryggestad E 2011 Small animal radiotherapy research platforms *Phys. Med. Biol.* **56** R55–83
Villarreal-Barajas E and Khan R F 2014 Energy response of EBT3 radiochromic films: implications for dosimetry in kilovoltage range *J. Appl. Clin. Med. Phys.* **15** 331–8
Wang Y-F, Lin S-C, Na Y H, Black P J and Wuu C-S 2018 Dosimetric verification and commissioning for a small animal image-guided irradiator *Phys. Med. Biol.* **63** 145001
Wong J *et al* 2008 High-resolution, small animal radiation research platform with x-ray tomographic guidance capabilities *Int. J. Radiat. Oncol. Biol. Phys.* **71** 1591–9
Yanch J C and Harte K J 1996 Monte Carlo simulation of a miniature, radiosurgery x-ray tube using the ITS 3.0 coupled electron-photon transport code *Med. Phys.* **23** 1551–8
Yasuda T, Beatty J, Biggs P J and Gall K 1998 Two-dimensional dose distribution of a miniature x-ray device for stereotactic radiosurgery *Med. Phys.* **25** 1212–6